DESIGN OF TOUGH HYDROGEL LUMENS FOR SIMULATING ARTERIAL PLAQUE

A Thesis

Presented to the Faculty of the Graduate School

of Cornell University

In Partial Fulfillment of the Requirements for the Degree of

Master of Science

by

Lihong Lao

August 2016

ABSTRACT

Presently, computational fluid dynamics (CFD) has been developed for modeling coronary artery pressure and flow, and predicting surgical outcomes for coronary artery disease (CAD). For accurate modeling, artificial arteries (phantoms) with synthetic plaque need to be produced and used for direct visualization of fluid through a stenosis.

This work presents a new approach to fabricate a synthetic phantom using tough hydrogels that have been selectively mineralized to mimic plaque formation, geometrically and mechanically. The occluded hydrogel lumens generated large pressure drops and commensurately lower flow rates compared with non-mineralized hydrogels. These effects could be tuned to comparable or more severe than natural arterial occlusions. Due to the similarity of our synthetic phantoms to natural ones, they are likely better simulations for coronary calcification than prior alternatives. They could be used as a learning tool for complementing CFD analysis, or as an *in vitro* system to develop interventional or implantable devices.

BIOGRAPHICAL SKETCH

Lihong grew up in Shaoxing County, Zhejiang Province, China. She received her Bachelor and Master of Science degrees in Polymer Science and Engineering from Zhejiang University in 2007 and 2010. Her master research was polymeric biomaterials for tissue engineering. She then spent four years working as a researcher in Dow Chemical Company, Shanghai Center. Eager to learn more deep fundamentals of chemistry and materials, she began the Materials Science and Engineering program at Cornell University in 2014. Since then, she has worked in Prof. Robert F. Shepherd lab on the project of synthetic hydrogel materials for simulating arterial plaque.

Dedicate to my parents, my sister and Xilin for giving me enormous support to my graduate study at Cornell University.

ACKNOWLEDGMENTS

This work was completed under the supervision of Prof. Robert F. Shepherd, and financially supported in part by Weill Cornell Medicine, under grant Nos. 5UL1TR000457-09 (NIH) and TL1TR000459 (NIH NCATS), and by the National Science Foundation Graduate Research Fellowship (DGE-1144153). The completion of this thesis owned the assistance of many parties.

First of all, deepest gratitude and appreciation to my academic chair, Prof. Shepherd for his patient guidance throughout this research. Without his expertise, knowledge and professional advice, this study would not be possible. Deep thanks also to Prof. Simon Dunham, Prof. Bobak Mosadegh, and Prof. James K. Min in Weill Cornell Medicine Center for generous guidance on paper writing. Since thanks also to Prof. Huiju Park for being my committee member, and for his valuable guidance and comment on thesis writing.

Sincere appreciation is also to many colleagues in Organic Robotics Lab. Special thanks to Sanlin S. Robinson for her sincere guidance on material preparation and testing, Huichan Zhao for her sincere help on designing and preparing 3D printed mold, Benjamin C. Mac Murray for his kind assistance and advice on setting up fluid test apparatus. Thanks also to Bryan Peele, Thomas J. Wallin, Shuo Li, Chris Larson and Ilse Van Meerbeek for their advice through the research.

This work made use of the Cornell Center for Materials Research Facilities supported by the National Science Foundation under Award Number DMR-1120296. I would also thank Philip Carubia and John Grazul for their assistance on materials and mechanical testing.

Last but not least, thanks also to my family and friends for the love and encouragement throughout this period.

TABLE OF PUBLICATION

- **Lihong Lao**, Sanlin S. Robinson, Bryan Peele, Huichan Zhao, Benjamin C. Mac Murray, James K. Min, Bobak Mosadegh, Simon Dunham, Robert F. Shepherd. Selective mineralization of tough hydrogel lumens for simulating arterial plaque. *Submitted to Advanced Healthcare Materials, 2016.*

TABLE OF CONTENTS

LIST OF FIGURES

1 Introduction

1.1 Cardiovascular Disease

Cardiovascular disease (CVD) is a class of diseases that involve the heart or blood vessels.[1] In 2010, CVD caused 788,000 deaths, more than one third of all deaths in the U.S. (**Figure 1.1**a).[2] Common forms of CVD are atherosclerosis, hypertension, blood-clotting disorders embolisms and thromboses, etc.[2] The most serious atherosclerotic diseases are coronary artery diseases (CAD), which is also called coronary heart disease (CHD), commonly known as a heart attack such as angina and myocardial infarction; it caused 380,000 deaths (the leading cause) in 2010 (**Figure 1.1**b and **Figure 1.2**).[1, 2] Other CVDs are stroke, hypertensive heart disease, rheumatic heart disease, cardiomyopathy, heart arrhythmia, congenital heart disease, valvular heart disease, carditis, aortic aneurysms, peripheral artery disease, and venous thrombosis.[1]

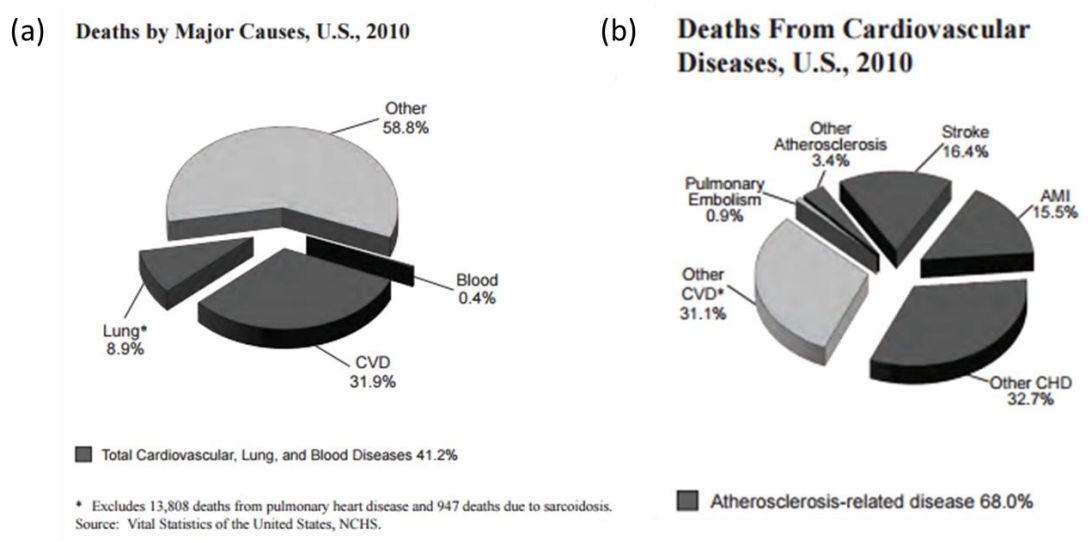

Figure 1.1 (a) Deaths by major causes, U.S., 2010, and (b) Deaths from cardiovascular diseases, U.S., 2010.[2]

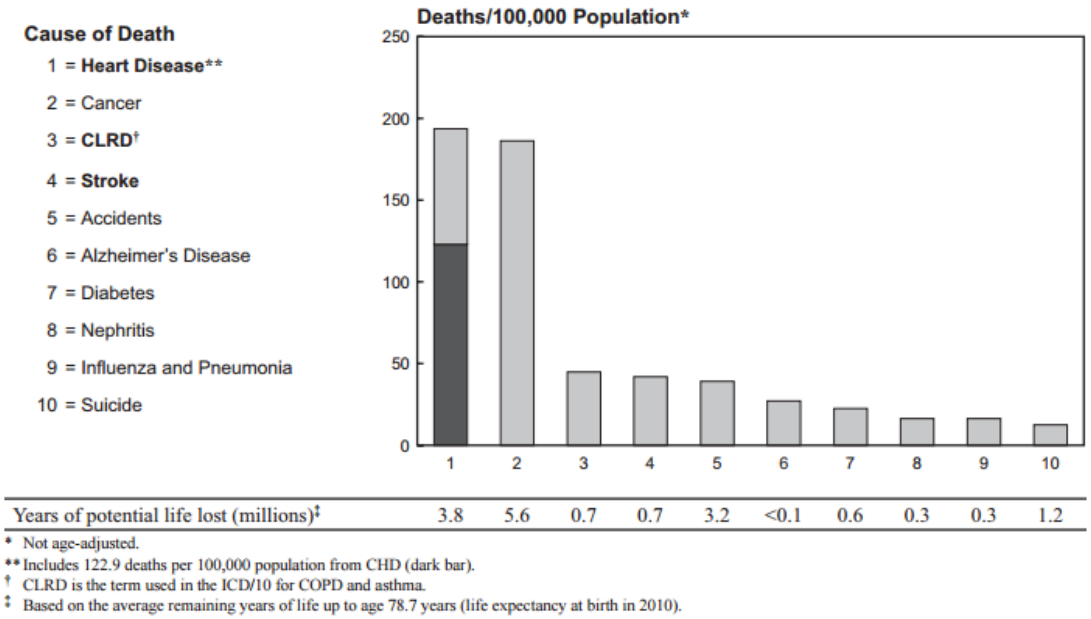

Figure 1.2 Ten leading causes of death: death rates, U.S., 2010.[2]

The annual number of deaths from CVD increased substantially from 1900 to 1970 in U.S.; since then, the trend has been slightly downward, but the number still remains high (**Figure. 1.3**).[2, 3] It continues to be the leading cause of death in U.S. and the world.

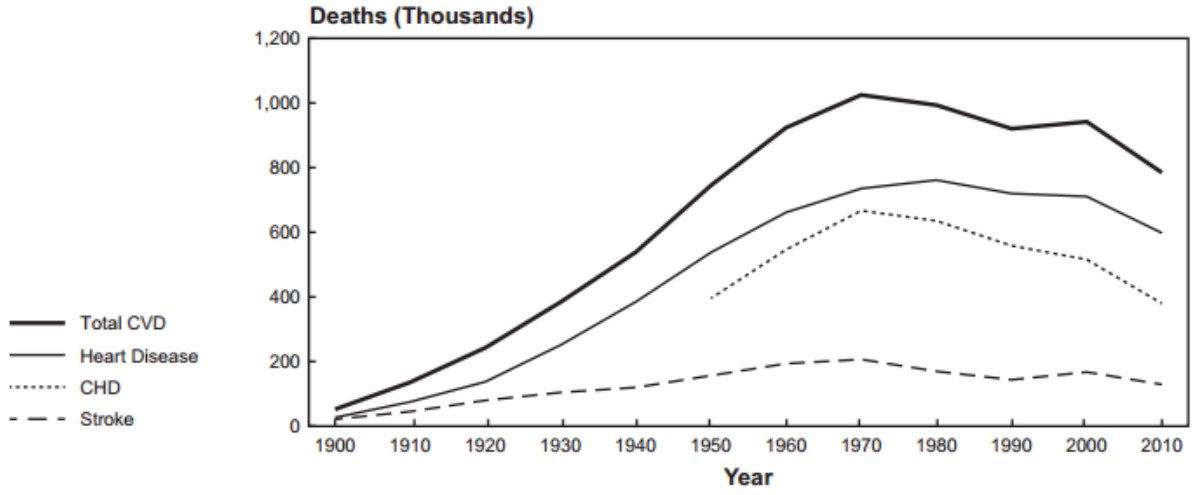

Figure 1.3 Deaths from cardiovascular diseases, U.S., 1900–2010.[2]

1.2 Coronary Artery Disease and Plaque

1.2.1 Coronary Artery Disease

Coronary heart disease (CAD) is a disease characterized by the buildup of plaque inside the coronary arteries, which is also called atherosclerosis. The buildup of plaque occurs over many years. Over time, it narrows coronary arteries, reduces blood flow, and thus oxygen perfusion to the myocardial tissue of the heart (**Figure 1.4**).[1, 4] Atherosclerosis can therefore lead to serious problems, including heart attack, stroke, or even death.[4]

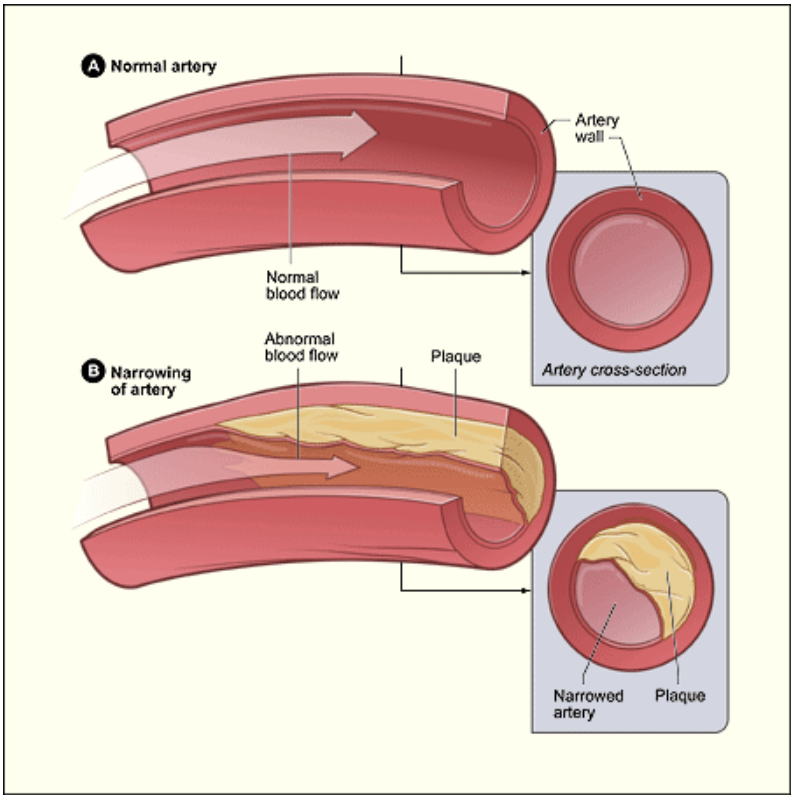

Figure 1.4 Illustration depicting the buildup of plaque in a coronary artery (atherosclerosis).[4] A shows a normal coronary artery with normal blood flow, and B shows a coronary artery narrowed by plaque with limited flow of oxygen-rich blood through the artery.

There are many risk factors for CAD, including growing age, diabetes, overweight, smoking, high blood pressure (hypertension), and high cholesterol, etc. Other factors such as sleep apnea, stress or alcohol may also raise the risk for the disease. Having atherosclerosis in other areas of the body, such as in the carotid or leg arteries (known as peripheral artery disease), also increases the risk of CAD.[4]

1.2.2 Plaque

1.2.2.1 Formation and Classification

Plaque is made up of fat, cholesterol, collagen, elastin and other substances found in the blood,[4] which may result from intimal proliferation of smooth muscle cells, or formation of fat and inflammatory cells inside the intima.[5-7] As plaque grows it accumulates scar (fibrous) tissue (**Figure 1.5**a).[8]

The fibrous caps in human atherosclerotic plaques are histologically classified to three types: cellular, hypocellular and calcified.[9] Cellular fibrous caps consist of smooth muscle cells (or other cells) and collagen or elastic fibers. Hypocellular fibrous caps consist of extracellular connective tissue matrix with rare cells. Calcified fibrous caps have abundant calcium (**Figure 1.5**b)[10] besides cells and fibers. Since crystallized calcium is hard, the plaque is often referred to as "hardening of the arteries".[5]

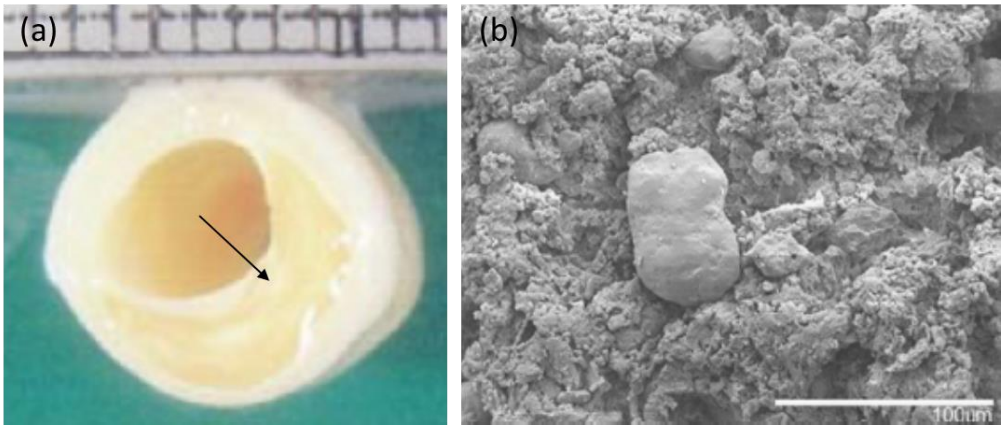

Figure 1.5 (a) Fibrous tissue (indicated as arrow) in atherosclerotic plaques of human iliac arteries (scale bar: one side of a square characterizes 1 mm),[8] and (b) Calcium phosphate crystals in human carotid calcified plaques (scale bar: 100 μm).[10]

Over time, plaque hardens or ruptures (breaks open). If the plaque ruptures, a blood clot can form on its surface. A large blood clot can mostly or even completely block blood flow through a coronary artery.[4]

1.2.2.2 Mechanical Properties

The mechanical and material properties of plaque are dramatically different than arterial tissues and they also differ from different plaque types.[11, 12] For instance, a dynamic compressive test has been conducted on 27 fibrous caps from human atherosclerotic aorta plaques, with stress amplitude of 0.5 kPa and frequency ranging from 0.05 Hz to 10 Hz. Although there was wide variability among samples, the mechanical difference among different plaque types was apparent, i.e. an average dynamic stiffness of 510±220 kPa for cellular plaque (compression level 17±6%) (**Figure 1.6**a), 900±220 kPa for hypocellular plaque (compression level 7±1%) (**Figure 1.6**b) and 2.27±1.0 MPa for calcified plaque (compression level 1.2±0.2%) (**Figure 1.6**c). The latter two were 1-2 times and 4-5 times stiffer than the first type, respectively.[9] Calcified plaque in human aortoiliac

tissue has also been reported with a dynamic stiffness values of 70 kPa at 5% compression and 1 MPa at 20% compression, respectively, similar with that of fibrous plaque and much higher than those of atheromatous tissue and healthy vessels.[13] Therefore, it was expected that different plaques respond differently to the same stenting procedure.[13]

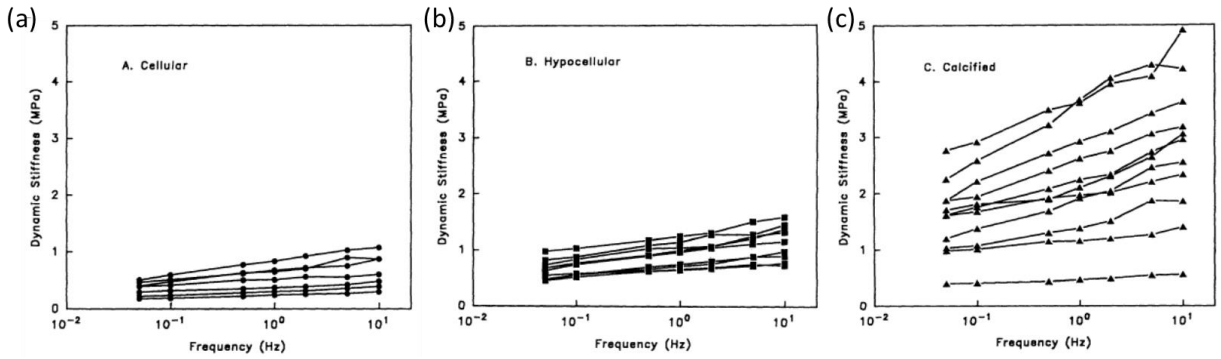

Figure 1.6 A prior report of amplitude (in MPa) of dynamic stiffness vs. frequency (in Hz) for (a) 7 cellular fibrous caps, (b) 9 hypocellular fibrous caps, and (c) 11 calcified fibrous caps in human atherosclerotic aorta plaques.[9]

Besides, mechanical behaviors of plaques vary from various testing conditions, e.g., dynamic or static loadings, tensile or compressive tests, etc.[9, 11, 12, 14, 15] For instance, a same group conducted a static uniaxial compressive test for similar human aortic plaque samples (as shown in **Figure 1.6**) under a loading of 8 kPa, and reported that non-fibrous samples has a compressive modulus of 41±18 kPa (under 24% compression strain), while that of fibrous and calcified plaques increased to 82±33 kPa (under 11% strain) and 355±245 kPa (under 3% strain), respectively. These values were about one order lower compared to those tested by dynamic loadings as shown in **Figure 1.6**. The difference was attributed to the non-elastic or visco-elastic mechanical behaviors of the tissues.[14] Though the three different plaque caps have statistically different mechanical properties under dynamic (**Figure 1.6**) or static compressive loading,[9, 14] they showed non-significant

differences under tensile loading.[16] Another review reported the stiffness of human plaques under static extension (kPa to GPa) was much higher than those under compression (kPa to MPa), although the values still varied in difference plaque sources (**Figure 1.7**),[11] which could be caused by the stiff collagen fibers carrying load only under tension.[15] In contrast, one of these studies did not find the difference between tension and compression properties for carotid plaques.[17]

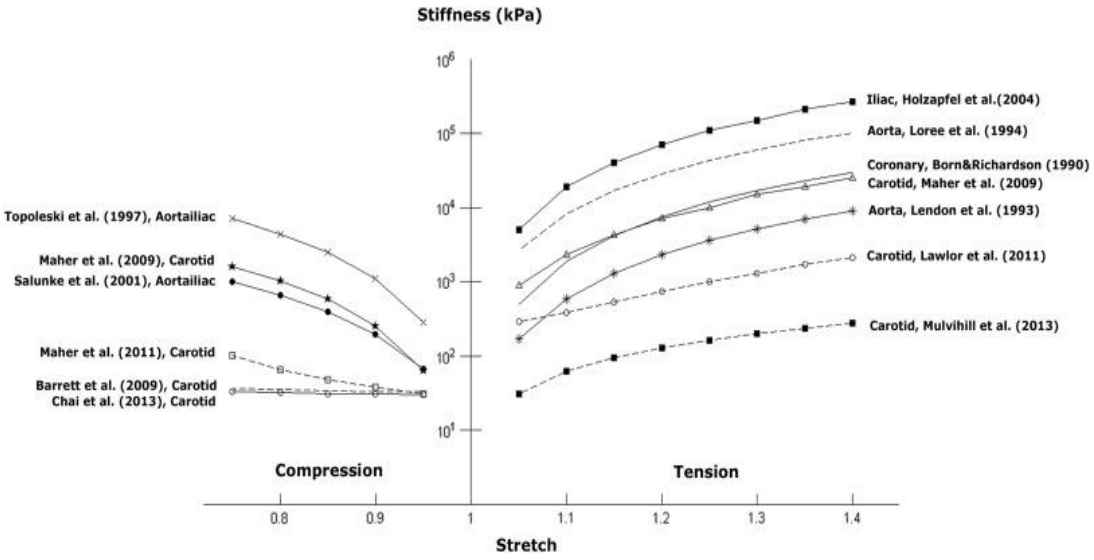

Figure 1.7 A prior review of tangential stiffness values for various plaques reported from the reviewed papers.[11]

1.2.3 Assessment Technologies

Both qualitative and quantitative assessment of how plaque grows and how blood flows through restricted pathways (stenoses) are used to assess the treatment of CAD in a patient. For example, computed tomography angiography (CTA) is as a non-invasive option for qualitative coronary imaging which now allows for acquisition of virtually motion-free images at isotropic spatial resolution of 400 μm (**Figure 1.8**a).[18, 19] However, using it alone has a limitation of

overestimation of stenosis severity, because stenosis observed by CTA is not necessarily associated with interruption of coronary artery blood flow and pressure.[19]

Fractional flow reserve (FFR) is a quantitative assessment adhered to imaging protocols (e.g. CTA), and uses a pressure wire to determine the ratio of maximal coronary blood flow through a stenosis to the blood flow in the hypothetical case for a normal artery (**Figure 1.8**).[19, 20] Therefore, the measurement reports the potential decrease of coronary flow in a diseased artery, and identifies a stenosis during coronary angiography and cardiac catheterization.[21] An FFR of 1.0 is widely accepted as normal; FFR value less than 0.75-0.80 was considered functionally significant and may need a surgery treatment for the disease. [19-21]

Due to the breadth and complexity of diagnostic tools, difficulty of patient access, and the variation in manifestations of the disease state itself, it is useful to assess the flow dynamics and the performance of diagnostic and therapeutic medicine in controlled settings. Towards that goal, computational fluid dynamics (CFD) modeling has been developed that allows for modeling of coronary artery pressure and flow (**Figure 1.8**c).[19, 22] Three-dimensional (3D) blood flow simulations are performed with blood modelled as a Newtonian fluid using incompressible Navier–Stokes equations with appropriate initial and boundary conditions using a finite element method on a supercomputer.[23] When CFD is added to standardly acquired CTA dataset, fractional flow reserve (FFR) derived from CTA (FFR_{CTA}) coronary map (**Figure 1.8**b) can be calculated by solving the equations of blood flow for the velocity and pressure fields, and then normalizing the mean hyperemic pressure field by the average mean hyperemic pressure in the aorta.[19] Using CFD for diagnostics, however, remains uncertain when assessing complex flow and pressure

calculations in plaque-laden arteries.[19, 24] Furthermore, simulating treatment or testing medical diagnostic tools cannot, presently, be done virtually.

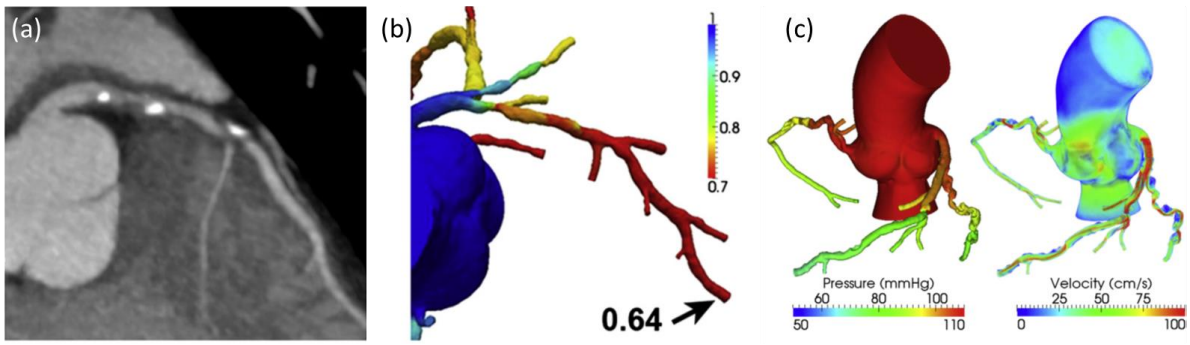

Figure 1.8 A prior report of (a) CTA demonstrating stenosis in the left anterior descending (LAD), (b) FFR_{CTA} demonstrates ischemia in the LAD, with a computed value of 0.64, and (c) CFD simulation of 3D pressure and velocity fields throughout the cardiac cycle across stenoses in the LAD, left circumflex (LCx,) and right coronary artery (RCA).[19]

1.3 Artificial Arteries (Phantoms)

For accurate modeling of CFD and as an alternative to measurements on patients, artificial arteries (phantoms) were produced and used for direct visualization of fluid through a stenosis.[25-31] Several prior designs have been composed of inorganic materials such as glass (**Figure 1.9**a),[25, 26] which do not match the material properties of soft tissues in real human arteries. Silicone-based elastomeric materials have also been widely used,[27-29] such as Elastrat Sarl (Switzerland) (**Figure 1.9**b),[28] to construct phantom models; however, the phantoms were usually mono-layered and single material, and therefore did not reproduce the wall architecture or chemistry present in plaque. Other attempts have also been made to directly print vascular phantoms by 3D Polyjet printers, using either hard (acrylic) or elastomeric materials (polyurethane) (**Figure 1.9**c).[30] In several cases, stenotic geometries were evaluated showing that these features will influence flow

and deformational mechanics of the arterial wall.[29, 31] While these studies highlighted the importance of the mechanics of the stenosis, the materials, silicones[29] and polyvinyl alcohol (PVA) (**Figure 1.9**d)[31] used were much softer than that of coronary calcium, which are orders of magnitude stiffer than healthy coronary tissue.[11] Ideally, these phantoms would represent a patient's specific arterial geometry, mechanics, and material properties for use in diagnostics and predicting the outcomes of invasive procedures.

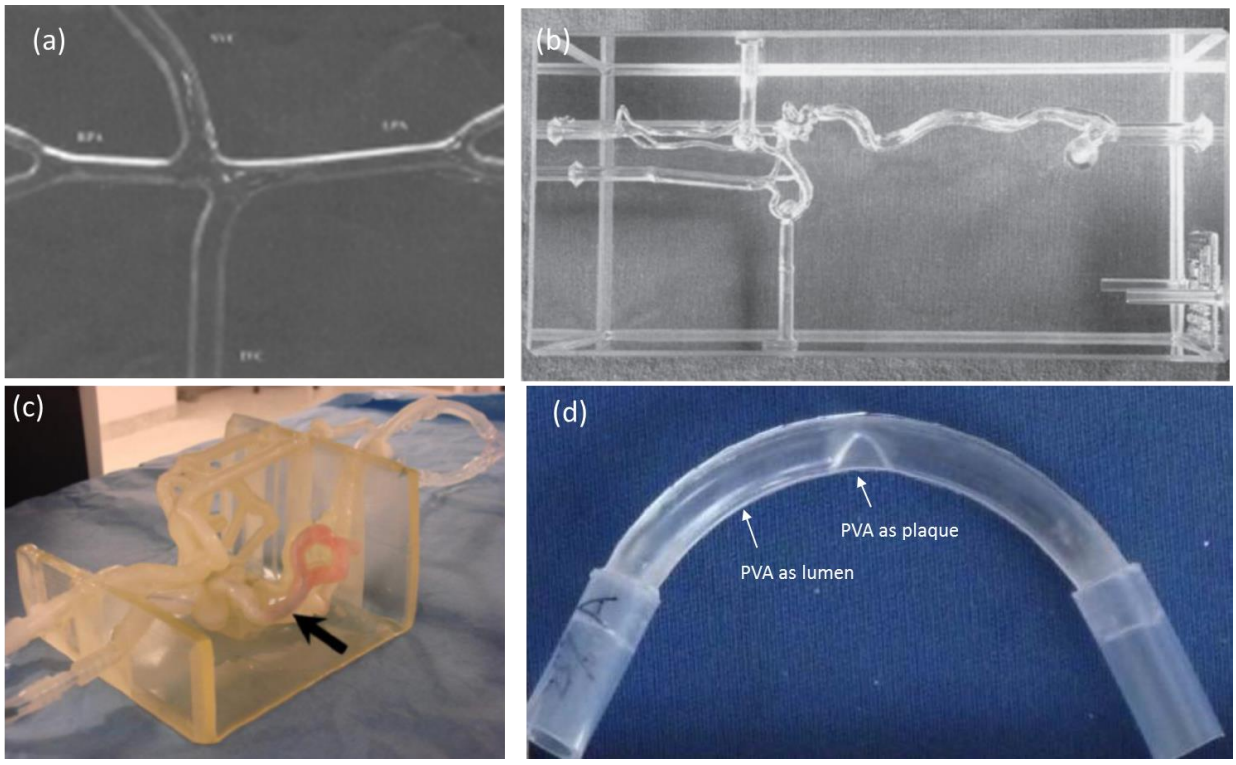

Figure 1.9 Prior designs of phantoms for coronary angiography. (a) Glass-blown Fontan phantom,[26] (b) Silicone-based phantom (company Elastrat Sarl),[28] (c) Acrylic-based phantom,[30] and (d) PVA hydrogel phantom.[31]

1.4 Objective and Design

In order to accurately simulate a patient's specific coronary arteries, we must be able to replicate both their shape and mechanical properties.[22, 23] Recently, hydrogels—swollen networks of hydrophilic polymer—have emerged as a viable material solution for mechanical devices.[32, 33] These hydrogel networks could provide support for liquid flow as a synthetic artery and have the potential for calcification to mimic the process of plaque formation that sometimes leads to CAD.

In this work, we aim at a new approach to fabricate synthetic artery phantoms using tough hydrogels that have been selectively mineralized to mimic plaque formation, both chemically and mechanically. We used transparent and tough polyacrylamide hydrogel as lumen and calcium crystals as plaque buildup (**Figure 1.10**). We reported compression tests to evaluate the mechanical properties of the calcified hydrogels, and image analysis of the calcium phosphate crystallization. Finally, we assessed the potential of these synthetic lumens to be used as arterial phantoms via fluid flow at the rates and pressures typical of the human cardiovascular system.

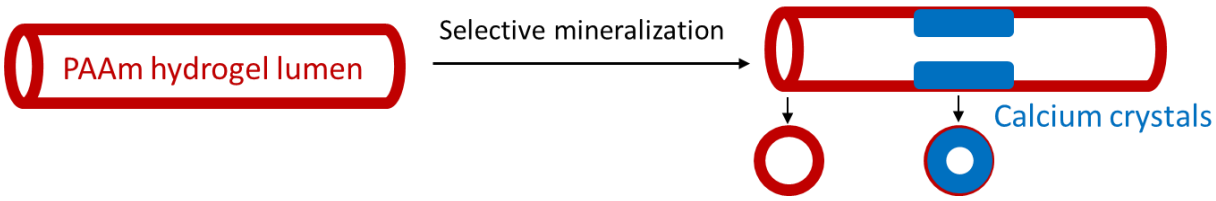

Figure 1.10 Scheme to show the design of synthetic artery phantoms using polyacrylamide tough hydrogels being selectively mineralized to mimic plaque formation.

2 Materials and Methods

2.1 Polyacrylamide Hydrogel

2.1.1 Hydrogel Preparation

The polyacrylamide hydrogels were synthesized using the following protocol.[33, 34] Acrylamide monomer (AAm; Sigma, A8887) was dissolved in deionized water, with AAm fixed at 2.2 M. The solution was subsequently mixed with a crosslinker, N,N′-methylene bisacrylamide (MBAA; Sigma, M7279) set at 0.01 the weight of AAm, a photoinitiator, Darocur® 1173 (BASF) was added at 0.15 wt% in solution, and ammonium phosphate dibasic ($(NH_4)_2HPO_4$; Sigma, 215996) was used at 0.4 M in solution. We stirred the solution overnight, at room temperature, until the solution was homogeneous and then poured it into a paper cup mold (diameter~62 mm, height~10 mm) with thickness of 3 mm and cured it via exposure to 365 nm light (350 W; OmniCure® S1500 A UV light curing system, Lumen Dynamics Group Inc) for 5 minutes. The sample was kept in a refrigerator (4 °C) overnight to ensure complete reaction and prevent drying.

2.1.2 Hydrogel Mineralization

To mineralize the hydrogels, we immersed them in a solution containing 0.4 M or 2 M calcium chloride ($CaCl_2$; Sigma, C1016) at room temperature.[34, 35] After 24 hours, the samples were extensively washed with deionized water to remove surface precipitates and immersed in a fresh solution containing $(NH_4)_2HPO_4$ with concentrations of 0.4 M or 2 M, respectively. We repeated these steps from one to four weeks for increasing degrees of mineralization (**Figure 2.1**). After the desired time, we washed the mineralized gels and wipe-dried the surface for further analysis.

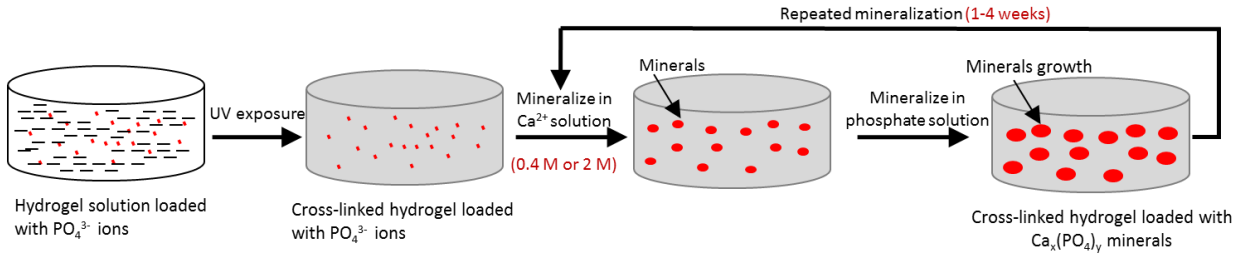

Figure 2.1 Scheme to show the photopolymerization of polyacrylamide (PAAm) hydrogel and repeated mineralization in 0.4 M or 2 M calcium and phosphate solutions.

2.1.3 Morphology Analysis

We used scanning electron microscopy (SEM) to observe the microstructure of the neat and mineralized PAAm hydrogel samples. To prepare the samples for the vacuum conditions of the SEM, we freeze dried them using liquid nitrogen.[36] We then coated the samples with a thin layer of gold palladium and observed them on a Tescan Mira3 FESEM. We used energy-dispersive X-ray spectroscopy (EDS) for elemental analysis.

2.1.4 Mechanical Test

We measured the mechanical properties of neat and mineralized hydrogels using dynamic mechanical analysis (DMA; TA Instruments, Q800) equipped with two parallel compression platens (12.7 mm in diameter). The samples were ~6.5 mm in diameter and ~3.0 mm in height (measured automatically via DMA software). We tested five parallel specimens for each set of samples. To obtain the dynamic storage moduli (E') of the hydrogels, the samples were compressed by preloading to 0.1 N contact force and applying a frequency sweep from 1 to 10 Hz using 0 to 2% compressive strain, $[L_0\text{-}L]/L_0$, where L_0 is original specimen length and L is ultimate specimen length. We also measured the stress vs. strain relationship in monotonic compression using the

DMA by preloading hydrogel samples to 0.1 N and compressing at a force ramp rate of 3 N min^{-1} with an upper force limit of 18 N. Compressive elastic moduli (E) were calculated from the 0 to 4% stress-strain curves.

We also tested fixed, human aortic tissue (cadaveric, Weill Cornell Medicine) in tension using DMA. To ensure the samples would not dry out during testing we equipped the instrument with a small chamber that we filled with saline solution. In addition, we modified the clamps of the DMA with sandpaper to better grip the tissue specimens. Using a #11 scalpel, we cut circumferential and longitudinal samples from a large rectangular aortic specimen (the original tubular specimen had already been opened when we received them). We applied a pre-load force of 0.1 N, and then performed a frequency sweep from 0.1 to 10 Hz. The sample along longitudinal and circumferential cut was notated as HA (LC) and HA (CC) on the DMA curve, respectively.

2.2 Selectively Mineralized Hydrogel Lumen

2.2.1 Lumen Preparation

Using polyacrylamide, we molded synthetic lumens by casting the acrylamide solutions into a transparent cylindrical mold (the inner diameter, outer diameter and total length was ~2.7 mm, 6.5 mm and 60 mm, respectively; **Figure 2.2**a). We then placed the molded lumens into a 3D-printed mold designed to isolate and selectively mineralize a segment of the hydrogel (**Figure 2.2**b). The three segment lengths (left, middle, and right) of the mold were 25 mm, 10 mm, and 25 mm, respectively. The middle section was initially filled with calcium chloride solution (0.4 M or 2 M) to mineralize the middle part of the lumen, the left and right sections were filled with deionized water. The joints of the mold assemblies were completely sealed by silicones (Ecoflex 00-30; Smooth-On Inc.) to avoid the calcium solution leaking from the inner region to the lumen

extremities. The mineralization was then repeated alternatively between phosphate and calcium solutions for up to four weeks.

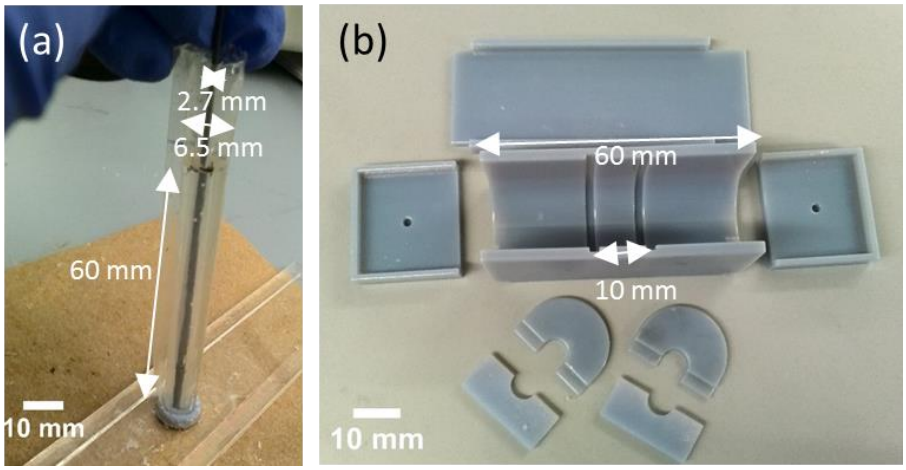

Figure 2.2 Images of (a) Transparent cylindrical mold with an inner tube for preparing PAAm hydrogel, (b) 3D-printed mold assemblies with three segments for selective mineralization for the hydrogel lumen.

2.2.2 Liquid Flow Test

We measured the hydraulic flux through the hydrogel lumens using a custom built flow apparatus (**Figure 2.3**). The difference (ΔP) between input (P_1) and output (P_2) pressures displayed in two pressure gauges (McMaster Carr, 3847K71) along the lumens was measured while the flow rate (Q) was gradually increased (measured using an Omega, FLDA3422G; with measurement range of 0 to 325 mL min^{-1}).[37]

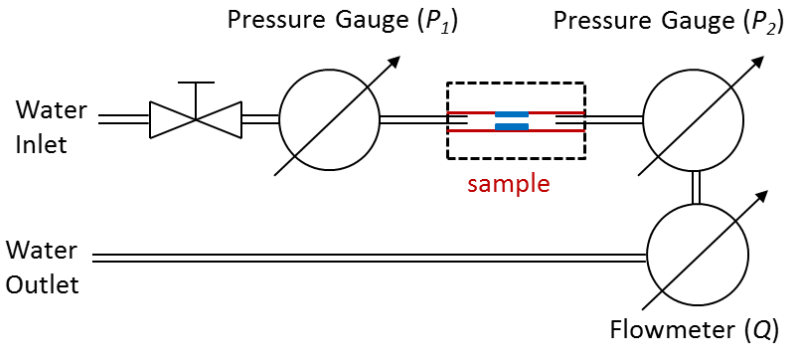

Figure 2.3 Scheme of a custom built apparatus for hydraulic flow test across PAAm hydrogel lumens.

2.3 Statistical Analysis

We analyzed the experimental data using ANOVA. The significance level was set as $p<0.05$. Results were reported as mean ± standard deviation.

3 Results and Discussion

3.1 Hydrogel Morphology

We synthesized mineral-incorporated polyacrylamide (PAAm) hydrogels via photopolymerization and repeated mineralization in 0.4 M or 2 M calcium and phosphate solutions (**Figure 2.1**) . **Figure 3.1** compares the SEM morphology of the bulk polyacrylamide hydrogels before and after repeated mineralization. The neat hydrogels showed a smooth and interconnected porous structure (**Figure 3.1**a), consistent with prior reports.[36, 38] The mineralized samples, however, transformed from transparent to white from light scattering due to surface roughening and an index of refraction mismatch between hydrogel and mineralized crystal growth (**Figure 3.1**b-f and Figure S1a, Supporting Information). The degree of crystallization and crystal morphology varied according to immersion time, t_c and solution concentration, $[Ca^{2+}]$.[35, 39] For short immersion times (one week) in low $[Ca^{2+}]$ concentrations (0.4 M), fine needle-like (acicular) crystals were formed along the pore walls (**Figure 3.1**b, indicated by arrows); Energy dispersive X-ray spectroscopy (EDS) confirmed that these crystals are calcium phosphate, as indicated by calcium (Ca) and phosphorus (P) elements (Figure S1b, Supporting Information). When it was further immersed in the solution, repeatedly for four weeks, the minerals grew into flake-like (platy) crystals with a higher density (**Figure 3.1**c). Increasing the ionic concentration of the solution to 2 M accelerated the mineral growth. As shown in **Figure 3.1**d, finer and denser minerals were found in the gel after one week compared with those mineralized in 0.4 M solution (**Figure 3.1**b). A still longer repeated incubation (four weeks) made minerals even denser, leading to a complete coverage of the gel by a thick layer of crystal needles (**Figure 3.1**e). The morphology was analogous with what has been observed in the prior reports,[34, 35] and coronary plaque with tissue calcification.[10]

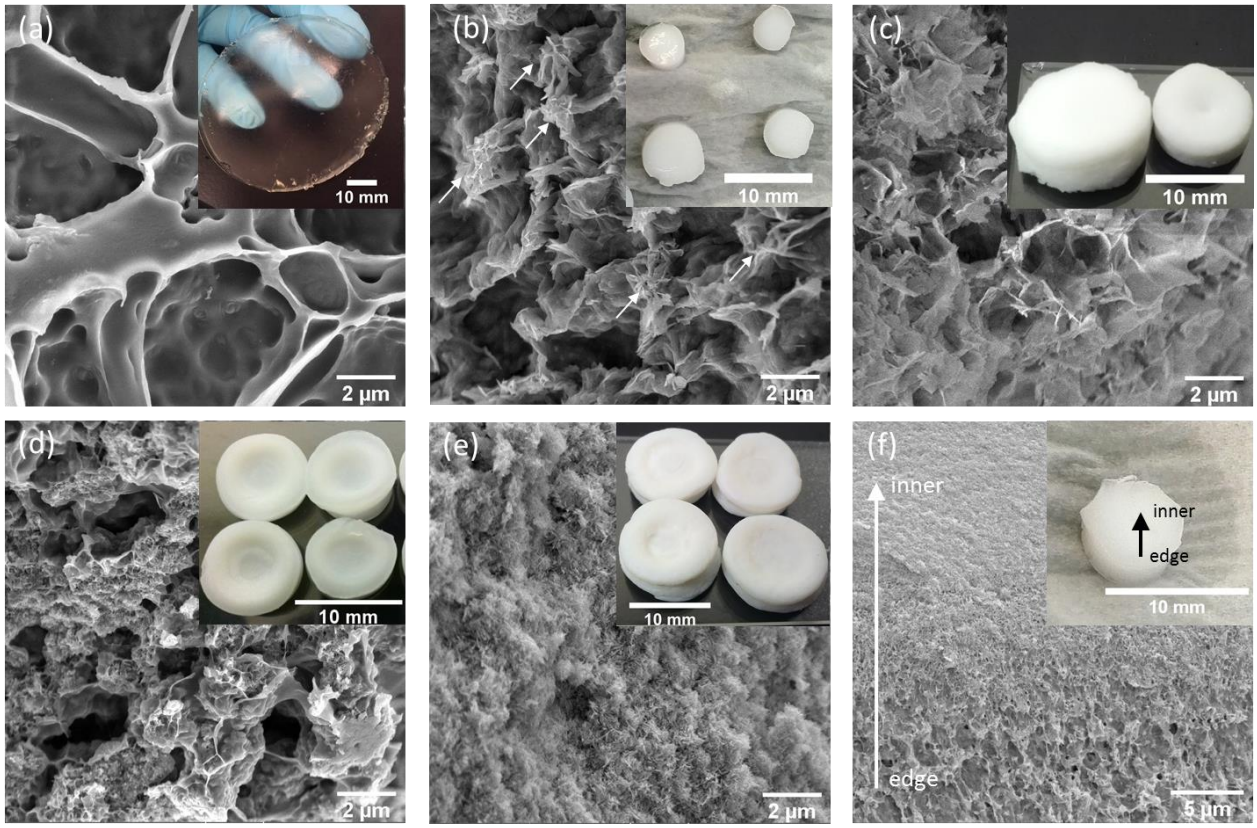

Figure 3.1 SEM morphologies of PAAm hydrogel loaded with phosphate ions (a) before and (b-f) after repeated mineralization in calcium and phosphate solutions under different conditions: (b) 0.4 M solution for 1 week, (c) 0.4 M solution for 4 weeks, (d) 2 M solution for 1 week and (e) 2 M solution for 4 weeks, respectively. (f) Cross section of mineral gradient from edge to inner of a hydrogel sample after mineralized in 0.4 M solution for 1 week. Insets are the sample images.

The increasing surface mineralization from the prolonged conditioning time is primarily due to surface nucleation on top of the already formed calcium phosphate crystals.[35, 39] We confirmed that the density of mineral on the interior of the gel is lower with a graded transition (**Figure 3.1**f and Figure S1a, Supporting Information), likely due to the mineralized surface reducing diffusive transport of ionic species.[35] The result is a gradient transition from a high elastic modulus mineral to a low elastic modulus hydrogel.

3.2 Mechanical Properties

Mechanical properties are an important characteristic for the plaque tissues during calcification.[11] Though plaque stretches circumferentially during blood pressure pulsation, it is also significantly compressed. Therefore, compressive tests are widely used to determine the mechanical behavior of atherosclerotic plaque tissues.[12, 40] To simulate the compressive mechanical properties of human arteries, we first measured the storage modulus (E') of healthy aortic tissue. Using dynamic mechanical analysis (DMA), we found a relatively frequency independent *E'* for healthy arteries that vary from E'~0.1 MPa to E'~2.5 MPa (**Figure 3.2**a). For example, in human artery 1 and 3, *E'* was higher along the longitudinal cuts (E'_{avg}~0.6 MPa and E'_{avg}~1.1 MPa, respectively) than by circumferential cut (E'_{avg}~0.1 MPa and E'_{avg}~0.5 MPa, respectively). Prior reports showed the dynamic moduli varied in different parts of human arterial tissues and in patients with different ages, e.g. ~0.5-3 MPa in carotid, thoracic and abdominal aortae,[41] ~0.5-7 MPa in iliac and femoral arteries,[41] and ~13.5 MPa for human aortic valve tissue.[42] Our results of healthy aortic tissues fall within these ranges.

Our synthetic hydrogel (PAAm) demonstrated a similar frequency insensitive storage modulus, with the pure PAAm having a E'_{avg}~29 kPa, well below that of fixed human arteries. When the gels were mineralized in a low ionic concentration ([Ca^{2+}]~0.4 M) for one week the storage modulus increased to E'_{avg} ~70 kPa, similar to the lower end of human arterial tissue. By controlling the immersion time (t_c) and ionic concentration ([Ca^{2+}]), we were able to tune the storage modulus of the synthetic hydrogel composite over the entire span of natural tissue. For example, increasing the ion concentration from 0.4 M to 2 M brought a significant increase of the dynamic modulus by ~75X in one week of mineralization (E'_{avg}~70 kPa vs. E'_{avg}~4.74 MPa,

significance level p<0.05), and extending the immersion time from one week to four weeks brought a ~150X increase in 0.4 M ion solution (E'_{avg}~70 kPa vs. E'_{avg}~9.37 MPa, p<0.05), and ~3X in 2 M ion solution (E'_{avg}~4.74 MPa vs. E'_{avg}~15.81 MPa, p<0.05), respectively.

The difference of the moduli between the four week mineralized hydrogel in the 0.4 M and 2 M solutions was insignificant (E'_{avg}~9.37 MPa vs. E'_{avg}~15.81 MPa, p>0.05), as demonstrated by the overlapping of the top two curves. Both mineralization processes resulted in significantly higher storage moduli than healthy human arteries (p<0.05; sample size, n=3).

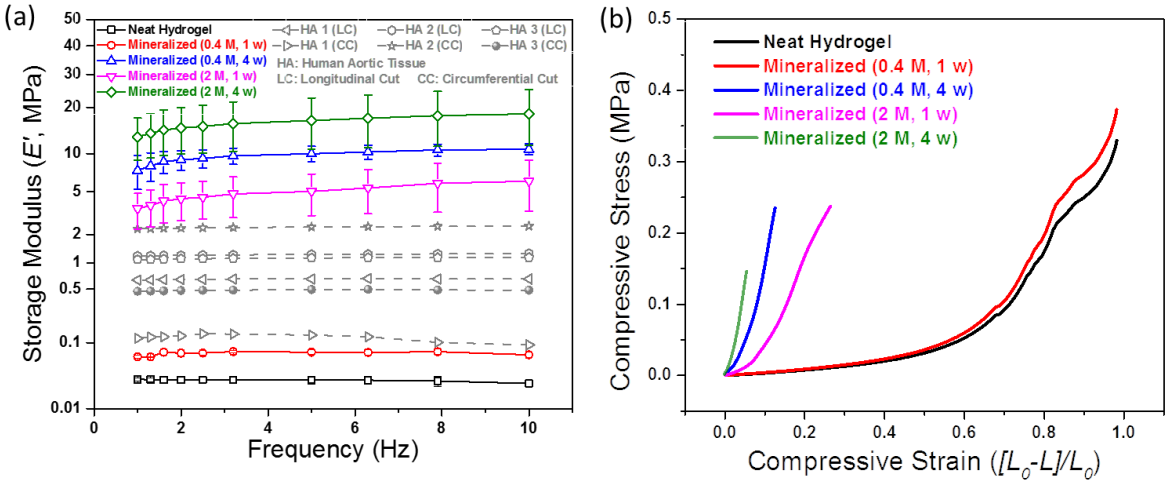

Figure 3.2 Mechanical properties tested via DMA for PAAm hydrogels before and after repeated mineralization under different conditions. (a) Storage modulus along with frequency sweep and (b) Compressive stress−strain curves. HA (LC) and HA (CC) stand for human aortic tissues with longitudinal and circumferential cut, respectively.

To determine what ranges of mechanical properties our synthetic materials can achieve, we performed monotonic compression tests over large strain ranges, as shown in **Figure 3.2**b. The neat hydrogel showed an elastic modulus, E_{avg} ~29 kPa, similar to that from the dynamic

frequency sweep (**Figure 3.2**a). Increasing both the ion concentration and mineralization time led to increased elastic moduli; however, the ultimate strain, ε_{ult}, was commensurately reduced. For example, samples mineralized in 0.4 M solution for four weeks had E_{avg}~2.2 MPa and ε_{ult}~0.13, and exposure to 2 M for four weeks resulted in a compressive storage modulus E_{avg}~2.4 MPa and ε_{ult}~0.06. As mentioned in Section 1.2.2.2, prior reports on the mechanical properties of plaqued arterial tissue yield highly variable results.[9, 11, 12, 14, 15] For compression tests on fibrous plaques, the moduli varied from 82±33 kPa (under 11% strain) for human aortic plaque,[14] to <10 kPa (under 5% strain) for human aortoiliac plaque;[43] for calcified plaques, the values varied from 355±245 kPa (under 3% strain) and 227 ± 34 kPa (under 10% strain) for human aortic plaque,[14, 40] 830 kPa (under 5% strain) and 13 MPa (under 20% strain) for human aortoiliac plaque,[43] to 140 kPa (under 5% strain) and 2.3 MPa (under 20% strain) for human carotid plaque,[15] respectively. These demonstrated our mineralized hydrogel has the potential to reach the stiffness of real human arteries with or without plaques under different controlled conditions.

3.3 Selectively Mineralized Lumen

Using a transparent cylindrical mold (**Figure 2.2**a), we prepared PAAm hydrogel lumens after UV curing. The lumens had an inner diameter, an outer diameter, and a total length of 2.74±0.15 mm, 6.48±0.20 mm and 60 mm, respectively (**Figure 3.3**a). The inner diameter was similar to the mean value of the real coronary arteries from patients with acute coronary syndrome imaged via intravascular ultrasound.[44] The selective mineralization was realized by immersing the middle region of the lumen in the mineralization solution (0.4 M or 2 M) while both ends were submerged in deionized water (**Figure 3.3**b), these fluids were renewed every 24 hours. **Figure 3.3**c shows a lumen after mineralization in 0.4 M solution for four weeks (images of samples with short t_c can

be found in Figure S2c,d, Supporting Information). We found the middle part calcified to completely white, while the sides remained transparent. The mineralization also occurred across the circumference of the lumen as indicated in **Figure 3.3**d (left). Additionally, we found a swelling of the non-mineralized portion of the lumen during mineralization, i.e. the total length increased to L~74 mm (**Figure 3.3**c), with the initial L_o~60 mm (**Figure 3.3**a and inner tube in **Figure 3.3**c); the circumferential wall also swelled and led to a higher expansion of the outer diameter (9.63±0.30 mm, ~48.6%) and shrinkage of the inner diameter (1.97±0.07 mm, ~28.1%) for the mineralized region (**Figure 3.3**d, left) compared with the non-mineralized sides (**Figure 3.3**d, right). In this view, an occlusion with ~33.0% nominal stenosis severity (the reduction of diameter)[31] has been selectively formed in the mineralized lumen.

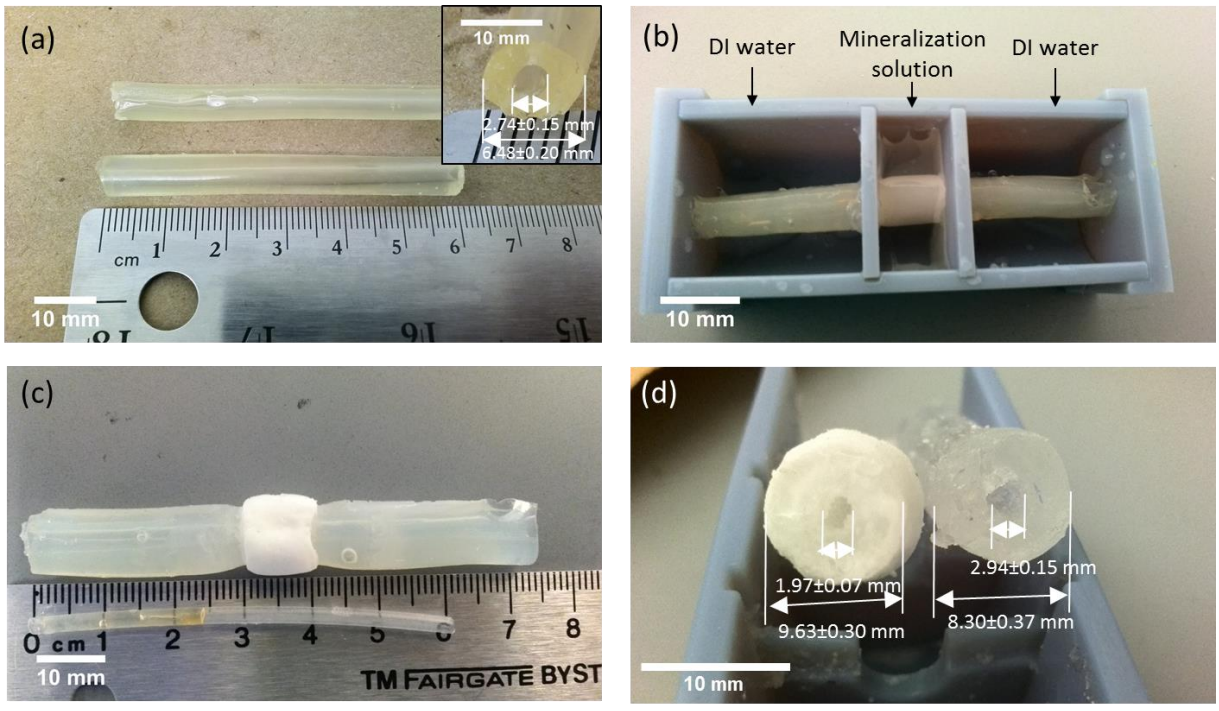

Figure 3.3 Images of PAAm hydrogel lumen before and after repeated mineralization. (a) As-prepared PAAm hydrogel lumen with the inset cross section image. (b) Hydrogel lumen sitting in the 3D-printed mold for selective mineralization. (c) Hydrogel lumen after mineralization in 0.4 M solution for 4 weeks,

compared with the original inner tube in the mold during curing. (d) Cross section view of the middle mineralized region (left) and non-mineralized region (right) within a same sample of (c).

3.4 Liquid Flow and Pressure

To demonstrate the potential application of the mineralized hydrogel lumen as a phantom for a plaque occluded artery, we set up a fluid flow system to test the pressures during flux through the lumens (**Figure 2.3**). We cut the samples into 50 mm long lumens with a 10 mm center section that we mineralized to various extents, and then inserted them into fittings (**Figure 3.4**a) connected to a water source. **Figure 3.4**b shows the difference (ΔP) between the inlet (P_1) and outlet pressures (P_2) through various hydrogel lumens with the water flow (Q) from $37.9<Q<252.4$ mL min^{-1}; we chose the maximum flow rate to approximate blood flow in the human internal carotid artery, $Q\sim250$ mL min^{-1}.[45, 46]

Overall, we found pressure drops across hydrogel lumens increased as the flow rate increased (**Figure 3.4**b), similar to measurements in natural arteries.[46] There was a strong correlation between the pressure drop, ΔP (P_2-P_1), across the lumen and degree of mineralization. The neat hydrogel lumen recorded a small $\Delta P\sim1.24$ kPa at the maximum flow rate. The one-week mineralization in 0.4 M solution did not bring significant difference in the pressure drop compared with the neat lumen ($p>0.05$), while the pressure driven flux for the gel mineralized in 2 M solution significantly deviated from that of the neat hydrogel at a higher flow rate (>150 mL min^{-1}; $p<0.05$). The drops were even more pronounced for lumens with a longer t_c of four weeks: under a maximum flow of 252.4 mL min^{-1}, the gel mineralized in 0.4 M solution generated a $\Delta P\sim5.58$ kPa, and the one in 2 M solution led to a $\Delta P\sim7.79$ kPa, about six times that of the non-mineralized neat sample.

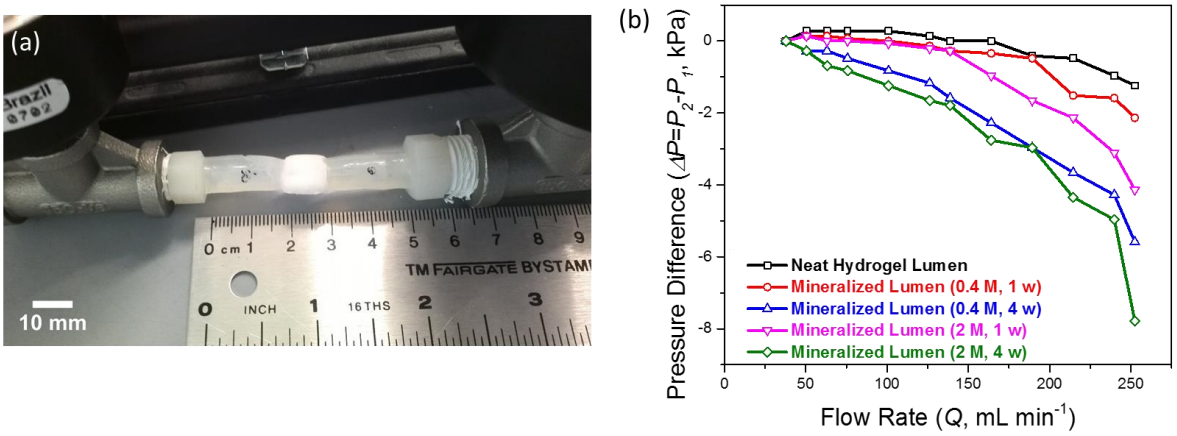

Figure 3.4 Water flow test across PAAm hydrogel lumens before and after repeated mineralization. (a) Image of a selectively mineralized hydrogel lumen sample connected within the flow system, and (b) Pressure difference across various hydrogel lumens with the increase of flow rate.

In our model, the pressure drop was generally produced due to the stenosis of the lumen.[47] The difference of mechanical toughness between the middle mineralized region and two non-mineralized sides also contributes to the flow rate across the lumen. When blood flows through a natural lumen it expands; however, stiff plaque prevents this expansive deformation and may generate a local pressure difference.[48, 49] For example, prior CFD simulations of blood flow through a 60% diameter-reducing stenosis has been reported to generate a pressure drop of 2.53 kPa (19 mm Hg) under a hyperemic flow of 216 mL min^{-1}.[19] Another simulation across a 10 mm long 67% diameter-reducing carotid artery stenosis has also been reported to generate pressure drops ranging from severe 7.73 kPa (58 mm Hg) to mild 1.60 kPa (12 mm Hg) depending on the positions and shapes of the distal end of the plaque, under a mean blood flow of ~250 mL min^{-1}.[46] **Figure 3.4**b demonstrates that our synthetic mineralization can achieve these features and be

appropriately used for phantoms to complement CFD analysis and aid in modeling and predicting surgical outcomes for CAD procedures.

4 Conclusion

In summary, we have developed a mineralized hydrogel system as a synthetic model for coronary arteries with plaque buildup. By tuning the mineral concentration, [Ca^{2+}], and crystallization time, t_c, we controlled the mechanical properties and degree of occlusion of the hydrogel lumens. The occluded lumen generated large pressure drops and commensurately lower flow rates compared with non-mineralized hydrogels; these effects could be tuned to comparable or more severe conditions than those related to natural arterial occlusions. Our preliminary results are comparable with a prior study, where a pressure drop of 1.3-10.7 kPa (10-80 mmHg) was tested with a flow rate of 30-210 mL min^{-1} along a synthetic stenosis model (with a higher nominal stenosis severity of 70%) made of PVA hydrogel as both lumen and occlusion.[31]

Due to the similarity of our synthetic material constituents to natural ones, these phantoms are likely better simulations for coronary calcification than previous alternatives. Since the mechanical properties of these hydrogel-based arteries mimic that of diseased ones *in vivo*, they could be used as a learning tool for clinical fellows to practice procedures (e.g., angioplasty, coronary artery bypass grafting (CABG), stent), or as an *in vitro* system to develop interventional or implantable devices. Furthermore, the molding technique allows these arteries to be fabricated in patient-specific geometries that will be useful for interventionalists and surgeons to plan for individual procedures.

5 Future Improvement

Future improvement of our synthetic lumens will better mimic the shape and exact material properties of patient specific arteries for improved phantom fidelity. For example, the hydrogel lumen could be better designed to mimic real artery, such as molding branched arteries,[27, 28, 30] of which 3D printing could be a good option.[30]

The flow test can be also adjusted to simulate real cardiac behavior, e.g. replacing water with blood formula for the pressure test, and applying a pulsatile flow.[27, 28] Specifically, while blood is a non-Newtonian liquid (density 1,060 kg/m^3, viscosity 0.004 Pa s), most CFD modeling requires Newtonian assumption.[19, 23, 45, 50] Though the testing fluid, water (density of 1,000 kg/m^3, viscosity 0.001 Pa s), meets the assumed behavior and has been used in prior studies,[31] its refractive index may not match with the hydrogel lumens and thereby may lead to optical perturbations inside the phantom in a further imaging process.[27, 28] To solve the problem, researchers used water-glycerol mixture (e.g. 55:45 v%, density 1,140 kg/m^3, viscosity 0.01017 Pa s, or 60:40 v%, density 1,114 kg/m^3, viscosity 0.0145 Pa s) to match the silicone phantoms.[27, 29] In larger arteries, the Newtonian model can provide a reasonable approximation for blood flow; however, in restricted flow regions (shear rate < 100 s^{-1}), non-Newtonian properties of blood become important.[50] A number of non-Newtonian models have also been developed for the rheological behavior of real blood.[51-54] For validation, a study added xanthan gum particles in water-glycerol mixture to mimic non-Newtonian shear-thinning properties and sodium chloride to further match the refraction index of the mixture to the silicone phantom, which led to a final density of has a density of 1,050 kg/m^3 and an infinite shear viscosity of 0.00447 Pa s; using shear-dependent Carreau-Yasuda model, they found an overall consistency between the measurement

and CFD simulation, expect discrepancies near the outflow of the model due to an effect of boundary condition.[28] A similar blood-analog fluid should be carried out in future work. Furthermore, to save the fluid, a circulation of fluid can be installed by using computer-controlled gear pumps.[27, 28, 31] This will also approximate the real pulsatile conditions found in the arteries.

Flow testing should also be performed on these materials using conventional medical imaging (e.g., CTA, echocardiogram, magnetic resonance imaging (MRI) and particle image velocimetry (PIV)) to assess their ability to simulate realistic tissue response and not just a time and position averaged flow response.[28-30]

Finally, though not shown in this work, it would be possible to accelerate the crystal growth and reduce the time required to cause the occlusion by further shortening the cycling time (t_c) and increasing calcium concentration ($[Ca^{2+}]$).

6 Supporting Information

Short-time Mineralization of Polyacrylamide Hydrogel

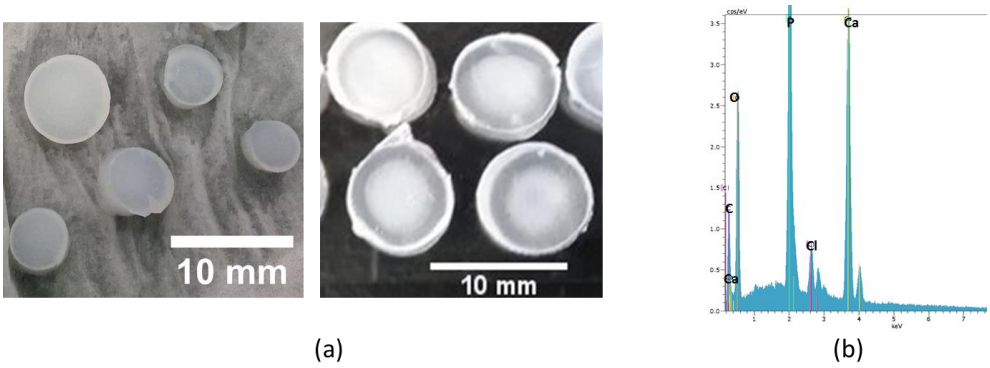

Figure S1 (a) Images of PAAm hydrogels loaded with 0.4 M phosphate ions after mineralization in (left) 0.4 M calcium solution and (right) 2 M calcium solution for 1 day, respectively. (b) Energy-dispersive X-ray spectrum (EDS) of PAAm hydrogels after repeated mineralization in 0.4 M calcium and phosphate solutions for 1 week.

Short-time Selective Mineralization of Hydrogel Lumens

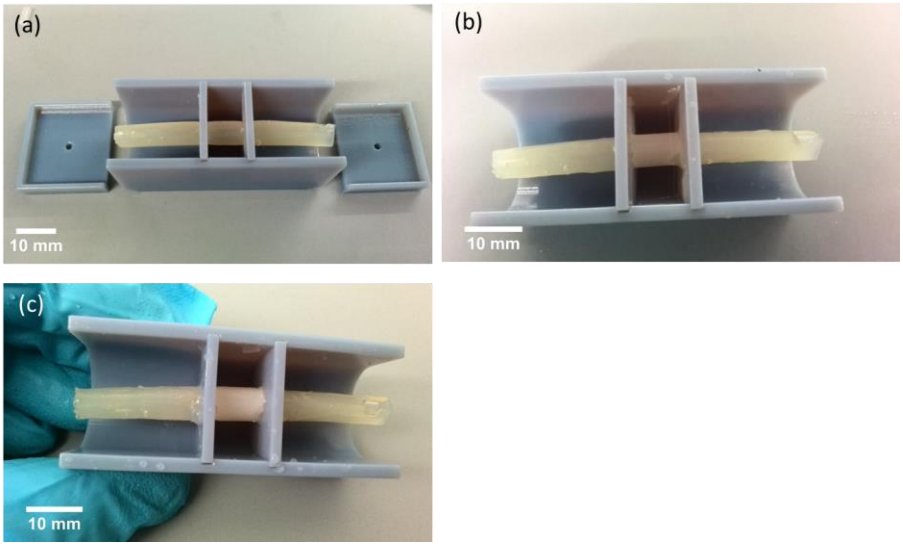

Figure S2. Images of (a) A neat lumen sitting in the mold before mineralization, (b) and (c) A lumen after selective mineralization in 0.4 M phosphate solution for 10 min and 1 day, respectively.

Reference

[1] S. Mendis, P. Puska, B. Norrving, World Health Organization, **2011**.

[2] NHLBI Fact Book, Fiscal Year **2012**.

[3] D. Mozaffarian, E. J. Benjamin, A. S. Go, D. K. Arnett, M. J. Blaha, M. Cushman, S. R. Das, S. de Ferranti, J. P. Despres, H. J. Fullerton, V. J. Howard, M. D. Huffman, C. R. Isasi, M. C. Jimenez, S. E. Judd, B. M. Kissela, J. H. Lichtman, L. D. Lisabeth, S. Liu, R. H. Mackey, D. J. Magid, D. K. McGuire, E. R. Mohler, 3rd, C. S. Moy, P. Muntner, M. E. Mussolino, K. Nasir, R. W. Neumar, G. Nichol, L. Palaniappan, D. K. Pandey, M. J. Reeves, C. J. Rodriguez, W. Rosamond, P. D. Sorlie, J. Stein, A. Towfighi, T. N. Turan, S. S. Virani, D. Woo, R. W. Yeh, M. B. Turner, C. American Heart Association Statistics, S. Stroke Statistics, *Circulation* **2016**, *133*, e38.

[4] http://www.nhlbi.nih.gov/health/health-topics/topics/atherosclerosis

[5] J. C. Kovacic, P. Moreno, E. G. Nabel, V. Hachinski, V. Fuster, *Circulation* **2011**, *123*, 1900.

[6] Y. S. Chatzizisis, A. P. Antoniadis, J. J. Wentzel, G. D. Giannoglou, *Atherosclerosis* **2014**, *236*, 351.

[7] M. R. Dweck, V. Puntman, A. T. Vesey, Z. A. Fayad, E. Nagel, *JACC Cardiovasc. Imag.* **2016**, *9*, 306.

[8] G. A. Holzapfel, G. Sommer, P. Regitnig, *J. Biomech. Eng.* **2004**, *126*, 657.

[9] R. T. Lee, A. J. Grodzinsky, E. H. Frank, R. D. Kamm, F. J. Schoen, *Circulation* **1991**, *83*, 1764.

[10] H. E. Barrett, E. M. Cunnane, E. G. Kavanagh, M. T. Walsh, *J. Mech. Behav. Biomed. Mater.* **2016**, *56*, 45.

[11] A. C. Akyildiz, L. Speelman, F. J. Gijsen, *J. Biomech.* **2014**, *47*, 773.

[12] C. K. Chai, L. Speelman, C. W. Oomens, F. P. Baaijens, *J. Biomech.* **2014**, *47*, 784.

[13] N. V. Salunke, L. D. Topoleski, J. D. Humphrey, W. J. Mergner, *J. Biomed. Mater. Res.* **2001**, *55*, 236.

[14] R. T. Lee, S. G. Richardson, H. M. Loree, A. J. Grodzinsky, S. A. Gharib, F. J. Schoen, N. Pandian, *Arterioscler. Thromb.: Vasc. Biol. / Am. Heart Assoc.* **1992**, *12*, 1.

[15] E. Maher, A. Creane, S. Sultan, N. Hynes, C. Lally, D. J. Kelly, *J. Biomech.* **2009**, *42*, 2760.

[16] H. M. Loree, A. J. Grodzinsky, S. Y. Park, L. J. Gibson, R. T. Lee, *J. Biomech.* **1994**, *27*, 195.

[17] M. G. Lawlor, M. R. O'Donnell, B. M. O'Connell, M. T. Walsh, *J. Biomech.* **2011**, *44*, 1709.

[18] P. Maurovich-Horvat, M. Ferencik, S. Voros, B. Merkely, U. Hoffmann, *Nat. Rev. Cardiol.* **2014**, *11*, 390.

[19] C. A. Taylor, T. A. Fonte, J. K. Min, *J. Am. Coll. Cardiol.* **2013**, *61*, 2233.

[20] W. B. Meijboom, C. A. Van Mieghem, N. van Pelt, A. Weustink, F. Pugliese, N. R. Mollet, E. Boersma, E. Regar, R. J. van Geuns, P. J. de Jaegere, P. W. Serruys, G. P. Krestin, P. J. de Feyter, *J. Am. Coll. Cardiol.* **2008**, *52*, 636.

[21] J. M. Daessle, *Soins* **2011**, S3.

[22] K. Govindaraju, I. A. Badruddin, G. N. Viswanathan, S. V. Ramesh, A. Badarudin, *Phys. Med.* **2013**, *29*, 225.

[23] Z. Sun, L. Xu, *Comput. Med. Imaging Graph.* **2014**, *38*, 651.

[24] B. K. Lee, *Korean Circ. J.* **2011**, *41*, 423.

[25] D. W. Liepsch, H. J. Steiger, A. Poll, H. J. Reulen, *Biorheology* **1987**, *24*, 689.

[26] M. Grigioni, A. Amodeo, C. Daniele, G. D'Avenio, R. Formigari, R. M. Di Donato, *Artif. Organs* **2000**, *24*, 946.

[27] A. Ugron, M. I. Farinas, L. Kiss, G. Paal, *Exp. Fluids* **2012**, *52*, 37.

[28] R. Bordas, S. Seshadhri, G. Janiga, M. Skalej, D. Thevenin, *Interv. Med. Appl. Sci.* **2012**, *4*, 193.

[29] J. Brunette, R. Mongrain, J. C. Tardif, *J. Visual.* **2004**, *7*, 241.

[30] C. N. Ionita, M. Mokin, N. Varble, D. R. Bednarek, J. P. Xiang, K. V. Snyder, A. H. Siddiqui, E. I. Levy, H. Meng, S. Rudin, *Proc. SPIE Int. Soc. Opt. Eng.* **2014**, *9038*.

[31] J. Ji, S. Toubaru, S. Kobayashi, H. Morikawa, D. L. Tang, D. N. Ku, *J. Biomech. Sci. Eng.* **2011**, *6*, 79.

[32] J. Y. Sun, X. Zhao, W. R. Illeperuma, O. Chaudhuri, K. H. Oh, D. J. Mooney, J. J. Vlassak, Z. Suo, *Nature* **2012**, *489*, 133.

[33] C. Keplinger, J. Y. Sun, C. C. Foo, P. Rothemund, G. M. Whitesides, Z. Suo, *Science* **2013**, *341*, 984.

[34] M. I. A. Joshy, K. Elayaraja, R. V. Suganthi, S. N. Kalkura, *Cryst. Res. Technol.* **2010**, *45*, 551.

[35] T. Yokoi, M. Kawashita, K. Kikuta, C. Ohtsuki, *Mater. Sci. Eng. C - Mater. Biol. Appl.* **2010**, *30*, 154.

[36] S. Kim, G. Iyer, A. Nadarajah, J. M. Frantz, A. L. Spongberg, *Int. J. Polym. Anal. Ch.* **2010**, *15*, 307.

[37] B. C. Mac Murray, X. An, S. S. Robinson, I. M. van Meerbeek, K. W. O'Brien, H. C. Zhao, R. F. Shepherd, *Adv. Mater.* **2015**, *27*, 6334.

[38] L. M. Lira, K. A. Martins, S. I. C. de Torresi, *Eur. Polym. J.* **2009**, *45*, 1232.

[39] L. H. Lao, Y. Zhu, Y. Y. Zhang, Z. Y. Gao, F. Zhou, L. K. Chen, H. W. Ouyang, C. Y. Gao, *Adv. Eng. Mater.* **2012**, *14*, B123.

[40] J. Walraevens, B. Willaert, G. De Win, A. Ranftl, J. De Schutter, J. V. Sloten, *Med. Eng. Phys.* **2008**, *30*, 1098.

[41] B. M. Learoyd, M. G. Taylor, *Circ. Res.* **1966**, *18*, 278.

[42] K. O. Lim, D. R. Boughner, *Circ. Res.* **1976**, *39*, 209.

[43] L. D. Topoleski, N. V. Salunke, J. D. Humphrey, W. J. Mergner, *J. Biomed. Mater. Res.* **1997**, *35*, 117.

[44] J. T. Schrauwen, D. J. Koeze, J. J. Wentzel, F. N. van de Vosse, A. F. van der Steen, F. J. Gijsen, *An. Biomed. Eng.* **2015**, *43*, 59.

[45] Z. F.Yang, H. T.Yu, G. P. Huang, R. Schwieterman, B.Ludwig, *J. Coast. Life Med.* **2015**, *3*, 245.

[46] B. K. Lal, K. W. Beach, D. S. Sumner, *J. Vasc. Surg.* **2011**, *54*, 1461.

[47] Z. Y. Li, J. H. Gillard, *J. Am. Coll. Cardiol.* **2008**, *52*, 499.

[48] A. Karimi, R. Razaghi, A. Shojaei, M. Navidbakhsh, *Biomed. Eng. - Biomed. Tech.* **2015**, *60*, 593.

[49] K. van der Heiden, A. Hoogendoorn, M. J. Daemen, F. J. Gijsen, *Thromb. Haemost.* **2016**, *115*, 501.

[50] D. M. Sforza, C. M. Putman, J. R. Cebral, *Annu. Rev. Fluid Mech.* **2009**, *41*, 91.

[51] W. L. Siauw, E. Y. K. Ng, J. Mazumdar, *Med. Eng. Phys.* **2000**, *22*, 265.

[52] J. R. Cebral, M. A. Castro, S. Appanaboyina, C. M. Putman, D. Millan, A. F. Frangi, *IEEE Trans. Med. Imaging* **2005**, *24*, 457.

[53] R. Manimaran. *Int. Sch. Sci. Res. & Innov.* **2011**, *5*,186

[54] J. P. Abraham, E. M. Sparrow, R. D. Lovik, *Int. J. Heat Mass Tranfer* **2008**, *51*, 5633.